DETECTING PATTERNS AND DRIVERS OF ICE ON AND ICE OFF TIMING IN ALASKAN RIVERS WIDER THAN 150 m USING MODIS

Wayana Dolan

A thesis submitted to the faculty at the University of North Carolina at Chapel Hill in partial fulfillment of the requirements for the degree of Master of Science in the Department of Geological Sciences.

Chapel Hill
2019

Approved by:

Tamlin M. Pavelsky

Laura J. Moore

Jonathan M. Lees

ABSTRACT

Wayana Dolan: Detecting patterns and drivers of ice on and ice off timing in Alaskan rivers wider than 150 m using MODIS
(Under the direction of Tamlin Pavelsky)

Annual river ice freeze-up and breakup have major implications for northern ecosystems and infrastructure and are particularly responsive to climate change. However, a lack of ground-based observations hampers understanding of large-scale patterns in ice timing. Here I detect freeze-up and breakup dates on Alaskan rivers wider than 150 m using MODIS satellite imagery from 2000-2017, the first large-scale detection of ice freeze-up using remote sensing and an expansion of breakup detection to rivers narrower than 500 m. I find statistically significant trends in breakup dates in the North Slope (-0.67 days/year, $p<0.05$) and West Central regions (-0.63 days/year, $p<0.10$). I find no long-term regional freeze-up trends. Regional timeseries of ice timing are instead dominated by teleconnections. Pacific Decadal Oscillation and Southern Oscillation Indices in the preceding fall and concurrent spring correlate highly to breakup dates, suggesting regional predictability. Methods described here can detect freeze-up and breakup timing on pan-Arctic rivers.

ACKNOWLEDGEMENTS

I thank my advisor, Dr. Tamlin Pavelsky, for his expertise, encouragement, and enthusiasm. His willingness to let me explore interesting conferences and participate in fieldwork, his lightning-fast editing, as well as the value that he places on his student's well-being, have made this process truly enjoyable. I also thank my committee members, Dr. Laura Moore and Dr. Jonathan Lees, for sharing different viewpoints and feedback on this project. Dr. Scott Lindsey provided ice on and ice off data for evaluation from the National Oceanic and Atmospheric Administration and Jeff Conaway at the United States Geological Survey shared insights about gage ice flagging.

I thank my lab mates, Angelica, Arik, Elizabeth, John, Madelyn, Matt, Melissa, Sarina, Shuai, Simon, Ted, and Xiao, for their friendship and research advice. A special thank you is given to Madelyn for providing food and moral support during the busy weeks and to Xiao for sharing his vast coding expertise, his willingness to discuss ideas about research, and his upbeat attitude. This degree wouldn't have been possible without my parents who encouraged me to study a topic that I am passionate about, even though it meant moving across the country. Nor would it have been possible without the support of Morgan, Paxton, and Britta on the West Coast who were willing to work with time differences to stay in touch. I also thank my roommate Justine for her understanding this past year and her cat Josie for a daily dose of positivity. Lastly, I thank the contra dance community in Chapel Hill for providing a home outside of academics.

TABLE OF CONTENTS

LIST OF FIGURES

LIST OF TABLES

LIST OF ABBREVIATIONS

DJF	December-January-February
ENSO	El Niño/Southern Oscillation
EPNP	East-Pacific/North-Pacific index
GRWL	Global River Widths from Landsat
JJA	June-July-August
MAE	Mean Absolute Error
MAM	March-April-May
MBE	Mean Bias Error
MERIT-DEM	Multi-Error Removed Improved-Terrain Digital Elevation Model
MODIS	Moderate Resolution Imaging Spectroradiometer
NIR	Near-Infrared
NWS	National Weather Service
PDO	Pacific Decadal Oscillation
PNA	Pacific North American pattern
RMSE	Root-Mean-Square Error
SOI	Southern Oscillation Index
SON	September-October-November
USGS	United States Geological Survey
VIIRS	Visible Infrared Imaging Radiometer Suite
WSC	Water Survey of Canada

DETECTING PATTERNS AND DRIVERS OF ICE ON AND ICE OFF TIMING IN ALASKAN RIVERS WIDER THAN 150 m USING MODIS

1. Introduction

River ice impacts an estimated 67% of rivers in the Northern Hemisphere (Yang et al., *in review*). During the winter, northern communities and industry rely on ice roads that transect or follow frozen rivers (Prowse et al., 2009). Diminishing ice thickness and duration impact the length of time during which ice roads can be safely traversed each year (Lonergan et al., 1993; Stephenson et al., 2011). Alternatively, a longer ice-free season creates new opportunities for shipping (Lonergan et al., 1993; Prowse et al., 2009). In addition to impacting transportation, ice breakup can instigate ice jam floods that damage near-river infrastructure (Rokaya et al., 2018). However, these ice jam floods are a dominant source of sediment and nutrients such as phosphorous, nitrogen, and carbon to near-river ecosystems including floodplains and deltas (Scrimgeour et al., 1994; Milburn & Prowse, 2000). Shifts in the duration of ice cover and severity of breakup are predicted to greatly influence these systems (Lonergan et al., 1993; Beltaos & Prowse, 2009; Prowse et al., 2009).

River ice breakup and freeze-up timing are responsive to changes in air temperature (Lacroix et al., 2005; Duguay et al., 2006; Prowse et al., 2007; Bennett & Prowse, 2010; Arp et al., 2013) and are therefore sensitive to climate change-induced warming. Using a ground-based dataset of long-term ice cover in Northern Hemisphere rivers and lakes, Magnuson et al. (2000) found that ice cover trended towards later freeze-up and earlier breakup over the past several centuries. In Canada, excluding the east coast, patterns in breakup timing based on ground observations

consistently trend towards earlier breakup (Lacroix et al., 2005; Duguay et al., 2006). Patterns in freeze-up are much less spatially consistent and depend greatly upon the years studied for trend analysis (Lacroix et al., 2005; Duguay et al., 2006).

In addition to long term trends, there is preliminary evidence to suggest a correlation between shorter term climactic variation and river ice breakup (Pavelsky & Smith, 2004; Bonsal et al., 2006; Bieniek et al., 2011). For example, the Pacific Decadal Oscillation (PDO) is a teleconnection that describes 20 to 30-year sea surface temperature patterns in the Pacific Ocean. During the warm phase, air temperatures in most of Alaska and Western Canada increase (Bieniek et al., 2012). Similar patterns are found for teleconnections associated with or impacted by the El Niño/Southern Oscillation (ENSO), such as the Pacific North American pattern (PNA) and the Southern Oscillation Index (SOI). Positive PNA anomalies usually associated with the El Niño phase of ENSO indicate warmer temperatures in most of Alaska and Western Canada, whereas positive SOI anomalies describing the La Niña phase of ENSO indicate cooler temperatures over the region (Bieniek et al., 2012). Bonsal et al. (2006) found that these indices strongly correlate to ice breakup dates, and to a weaker extent, freeze-up dates in the western parts of Canada. Pavelsky and Smith (2004) found the same correlation between PDO and earlier ice breakup in the Mackenzie River in Canada, but opposite correlations for two large Siberian rivers. However, not all studies agree about which teleconnections have the most influence on ice breakup timing. Schmidt et al. (2019), analyzing the Global Lake and River Ice Phenology Database (Benson et al., 2000), found no strong correlations between PDO and breakup, but noted that positive PNA anomalies were strongly related to earlier breakup in Canada. The East-Pacific/North-Pacific (EPNP) pattern is a spring-summer-fall mode of variability in pressure heights over Alaska/Western Canada and the North Pacific/Eastern United States that may also

impact river ice due to its positive correlation to Alaskan air temperature (Bieniek et al., 2012). Sea ice area influences Arctic precipitation (Sewall, 2005; Kopek et al., 2016), and therefore may indirectly impact river ice formation and breakup.

The influence of both long-term and short-term climate patterns on river ice have been, with the exception of Pavelsky and Smith (2004), studied using point-based ground observations. However, ground-based observations are limited in number, have greatly declined since a peak in the 1980s (Shiklomanov et al., 2002; Lacroix et al., 2005), and are not always representative of how river ice behaves along entire rivers (Cooley & Pavelsky, 2016).

One solution to this problem is to study trends in river ice freeze-up and breakup dates using remote sensing. This approach allows researchers to identify how ice changes throughout entire river systems. Previous papers use optical remote sensing to detect river ice breakup on individual rivers (Pavelsky & Smith, 2004; Chaouch et al., 2014; Chu & Lindenschmidt, 2014; Gauthier et al., 2015; Cooley & Pavelsky, 2016; Muhammad et al., 2016). Pavelsky and Smith (2004) used the MODerate resolution Imaging Spectroradiometer (MODIS) and the Advanced Very High-Resolution Radiometer to visually identify breakup on four large (> 500 m wide) Arctic rivers, the Lena, the Ob, the Mackenzie, and the Yenisey. Cooley & Pavelsky (2016) created a stationary threshold-based automated ice detection algorithm for the same four large rivers, also using MODIS. This method works well for wide rivers where river-observing pixels do not also contain areas of land. However, stationary reflectance thresholds produce inaccurate results in narrow (< 500 m) or braided rivers because of the high incidence of mixed pixels.

To address this issue, Chaouch et al. (2014) created a multi-threshold decision tree approach to classify river pixels on the Susquehanna river as pure water or mixed land/water. They then further classified the state of pixels in those categories as ice, mixed water/ice, or water, but did

not calculate breakup or freeze-up dates. Based upon these methods, the National Oceanic and Atmospheric Administration has implemented a real-time ice state detection approach on rivers in Alaska using the Visible Infrared Imaging Radiometer Suite (VIIRS). While the algorithm is applied to sub-VIIRS pixel rivers, it is primarily geared towards real-time ice state detection of individual pixels, does not include calculations of breakup and freeze-up dates, and is not available for historical trend analysis. The only previous study focused on remotely sensed freeze-up timing detection (Chu and Lindenschmidt, 2014) used MODIS imagery to detect ice phenology on several reaches of the Slave River in Canada. While this study demonstrates the feasibility of using optical imagery to detect ice freeze-up, no studies have applied detection methods on larger spatial scales.

In this thesis, I present a new method that uses MODIS data to observe ice freeze-up and breakup timing on all rivers wider than 150 m in Alaska and the Canadian portion of the Yukon River Basin. Using this dataset, I complete a regional analysis to better understand long-term trends as well as climatic drivers of interannual variability in ice timing. This research represents the first study of statewide trends in river ice phenology in Alaska.

2. Methods

2.1 Datasets

Launched in 1999 on the Terra Satellite, MODIS has a viewing swath of 2,330 km and provides daily imagery over the entire study area. I use three MODIS products for this analysis, including 250 m resolution daily red band (620-670 nm) imagery included in the MOD09GQ.006 product (Vermote et al., 2015a), the 'state_1km' band from the daily MOD09GA.006 product (Vermote et al., 2015b), and the temporally stationary MOD44W.005 water mask (Carrol et al., 2009). This analysis focuses on the time period between February

2000, when MODIS data first became available, through December 2017. While MODIS's spatial resolution of 250 m limits the size of observable rivers, the daily temporal resolution allows for the study of rapid events such as freeze-up and especially breakup, which are otherwise unobservable in finer spatial-scale imagery, such as Landsat 5-8, available over the same time period. All MODIS data is accessed through Google Earth Engine.

I analyze all river reaches in the Global River Widths from Landsat (GRWL) simplified vector product (Allen & Pavelsky, 2018) with median widths larger than 150 m within Alaska and the Canadian portion of the Yukon River Basin. While 150 m is narrower than a MODIS pixel, ice-driven seasonal patterns in reflectance, in which ice corresponds to high reflectance and water corresponds to low reflectance, are still present. The GRWL simplified vector product divides the original point-based GRWL database into reaches in which each reach is approximately between tributary junctions. The length of GRWL reaches are, therefore, highly variable. Cooley & Pavelsky (2016) demonstrate the feasibility of ice breakup detection within reaches of approximately 10 km in length (Cooley & Pavelsky, 2016). As a result, GRWL reaches longer than 10 km are divided into segments of approximately 10 km in length, for a total of 1149 reaches with a cumulative length of ~12,355 km.

Additionally, for analysis of trends and regional patterns, I divide the study rivers into seven regions based upon groups of Level 6 HydroBASINS (Lehner & Grill, 2013) and prior knowledge about the geography and climate of Alaska (**Figure 1**). These regions are the North Slope, West Central, Southwest (SW) Yukon, Central Yukon, Southeast (SE) Yukon, Southwest, and Southeast. Within these regions, I analyze the correlation of freeze-up and breakup dates to the PDO (Mantua et al., 1997; acquired from http://research.jisao.washington.edu/pdo/PDO.latest.txt), the PNA (Wallace & Gutzler, 1981;

Barnston & Livezey, 1987; acquired from ftp://ftp.cpc.ncep.noaa.gov/wd52dg/data/indices/pna_index.tim), the EPNP (Barnston & Livezey, 1987; Bell and Janowiak, 1995; acquired from ftp://ftp.cpc.ncep.noaa.gov/wd52dg/data/indices/epnp_index.tim), and the SOI (Trenberth, 1976; acquired from https://www.ncdc.noaa.gov/teleconnections/enso/indicators/soi/data.csv). I also compare breakup and freeze-up dates to regional sea ice area measurements from the Bering Sea, the Chukchi Sea, and the Beaufort Sea (Meier et al., 2007; Fetterer et al., 2017; acquired from: ftp://sidads.colorado.edu/DATASETS/NOAA/G02135/seaice_analysis/).

Data used for evaluating the accuracy of results includes ice flags from United States Geological Survey (USGS) and Water Survey of Canada (WSC) gage stations, MERRA-2 daily surface air temperature data (M2SDNXSLV, Global Modeling and Assimilation Office, 2015), and visual observations of ice on and ice off from the National Weather Service's (NWS) Alaska-Pacific River Forecast Center (breakup data available at: https://www.weather.gov/aprfc/breakupMap; freeze-up data available at: https://www.weather.gov/aprfc/freezeUp). I also use the 3" resolution Multi-Error Removed Improved-Terrain DEM (MERIT-DEM) (Yamazaki et al., 2017) to assess the risk of noise-causing topographic shadow near each river reach.

2.2 Ice breakup & freeze-up date detection algorithm

First, river-observing pixels are extracted from MOD09GQ.006 daily imagery. I create a river mask by using cumulative cost mapping, a tool that distinguishes river pixels from miscellaneous water pixels in the MOD44W.005 water mask. Cumulative cost mapping selects pixels in the water mask that either intersect river centerlines or border pixels which intersect

centerlines within 5 km (**Figure 2a**). This river mask is then applied to each daily MODIS image.

To remove pixels that are influenced by clouds, I use the 'state_1km' band from temporally coincident MOD09GA.006 observations. The band has sixteen bits that represent each pixel's state. Bits related to clouds include cloud state (bits 0-1), cloud shadow (2), cirrus detected (8-9), an internal cloud algorithm flag (10), and a pixel adjacent to cloud flag (13). I find that the cloud state flag (bits 0-1) is sufficient for this analysis. Other bits often over-filter cloud-free pixels, making breakup and freeze-up detection challenging.

Freeze-up and breakup timing are calculated on a reach-by-reach basis. Therefore, the haversine distance function (Sinnott, 1984) is used to match each river pixel to its nearest centerline. Reaches containing 10 or fewer pixels are not included in further analysis. For the remaining reaches on each date, I calculate the percentage of cloudy pixels and the hours of sunlight that the pixels experience based upon latitude and date (Hijmans et al., 2017). Observations with greater than 50% clouds are removed from analysis.

Topographic and cloud shadows can also cause noisy reflectance values. To lessen the impact of this noise, the standard deviation of topography within 2 km of each reach's centerline is calculated using MERIT-DEM. If the standard deviation of topography for a reach is greater than 200 m, I remove dates from analysis when pixels experience less than 10 hours of sunlight. For moderate topographic variation areas (100 m-200 m), observations with less than 8 hours of sunlight are removed. For all other reaches, observations with less than 6 hours of sunlight are filtered from analysis. Additionally, MODIS imagery in January in northern latitudes is often of poor quality due to polar night effects. Therefore, for pixels above 60° north, the month of

January is excluded from analysis. In future work, I will update methods to more accurately reflect low light conditions by removing dates within two weeks of December 21st.

Once cloudy and shadow-prone pixels are removed, I create a reach-specific reflectance threshold to differentiate between ice and water pixels. Previous studies used the near-infrared (NIR) band to detect river ice because of the difference in reflectance between water and ice in the NIR wavelengths (Cooley & Pavelsky, 2016). The widths of many of the rivers in this study are near or below MODIS resolution. Therefore, many pixels are not pure water pixels because they contain vegetation. The NIR band is very sensitive to the presence of vegetation (Colwell, 1974; Huete et al., 2002), which makes NIR band freeze-up and breakup detection challenging. I find that the red band is highly sensitive to the differences in reflectance between ice and water but is not nearly as sensitive to vegetation. To create a reach-specific threshold, I create a density plot of the red band reflectance of all the pixels that observe a reach during the months of January through July. The distribution of reflectance is bimodal during this time period, with ice pixels having high reflectance and water pixels having low reflectance. The reflectance of the antimode of the density plot becomes the reach-specific threshold (**Figure 2b**). To ensure accurate ice detection, I exclude cases in which the detected reflectance threshold is between 0.1 and 0.5 and in which <10% of pixels fall into the ice category. These cases occur in extremely cloudy areas that lack observations of river ice during the winter and spring.

Using this reach-specific threshold, I calculate the fraction of pixels ice covered for each reach on each date, referred to as the ice fraction. Occasionally, there are ice fraction spikes due to clouds that were not properly removed during the ice-free season or pits during the ice-covered season caused by incorrectly filtered cloud shadows (**Figure 2c**). To filter out spikes and

pits, observations are removed on dates that have an ice fraction more than 25 percentage points different from both the previous and next consecutive observations.

To calculate freeze-up and breakup dates for each year, I use an 'ice year' starting on day of year 213 (Aug 1st on non-leap years) to allow for freeze-ups that occur after the first of the new calendar year. For example, ice year 2013 refers to Aug 1st, 2012 through July 31st, 2013. I do not detect freeze-up for ice year 2000 because MODIS data only became available at the end of February in 2000. For all other ice years, I count the number of consecutive dates above an ice fraction of 0.2 (ice observations) and below an ice fraction of 0.2 (water observations). If there are fewer than 3 consecutive observations of ice in an ice year's timeseries, a freeze-up date is not calculated. Otherwise, I identify the start of the first ice-covered period containing 3 or more observations. The calculated freeze-up date is the date halfway between the start of the first ice-covered period and the previous open water observation (**Figure 2c**).

To calculate the breakup date, I analyze only ice fraction observations occurring after the freeze-up date. Therefore, if no freeze-up date is calculated in a given ice year, no breakup date will be calculated. Additionally, breakup dates are not calculated for ice year 2018 because the data stops on December 31st, 2017. The breakup date is the date halfway between the end of the final ice-covered observation in each year and the next available open water observation. Once the freeze-up and breakup dates are calculated for all years for a given reach, I flag observations if the uncertainty in the measurements (the half-distance between the low-cloud observation preceding the ice on/off date and the next low-cloud observation following the ice on/off date) is greater than ±10 days (**Figure 2c**). Data flagged with high uncertainty is not used in the trend and pattern analysis described in following sections.

2.3 Evaluation methods

I evaluate ice phenology time series using *in situ* observations from the USGS, WSC, and the NWS. This process is described as evaluation rather than validation because point-based field observations and reach-based remote sensing measurements are fundamentally mismatched in scale. First, I compare MODIS-derived ice fractions to USGS daily discharge flags at 26 gage locations (**Figure 1**). This analysis is supplemented with observations from 128 WSC gages and calculate MODIS ice fractions for nearby Canadian river reaches. The USGS flags daily discharge as estimated ('e'), which, for Alaskan rivers, usually corresponds to when the stage-discharge relationship is impacted by ice or, occasionally, flooding (River Ice Processes, 2017). WSC flags daily discharge observations ('B') if the stage-discharge relationship is influenced by ice. However, WSC and USGS ice flags are not present for daily discharge observations of several rivers in certain years when the rivers definitively freeze (based upon geographic location and visual inspection of high-resolution Landsat 5-8 imagery and Sentinel-2 imagery). Therefore, to remove these observations from evaluation, MERRA-2 average daily surface air temperature is used to calculate the mean air temperature for the 30 days prior to each WSC or USGS observation. While river ice dates are strongly correlated to 0° isotherm days (Bennett & Prowse, 2009; Prowse et al., 2010), to be conservative, I filter out any USGS or WSC daily observations not flagged as ice when the previous 30 day mean air temperature was below -3° Celsius. Once the gage-derived ice flags have been filtered, ice flags are created for the daily MODIS ice fractions. Days with ice fractions larger than 0.25 are flagged as ice, and days when the ice fractions are less than 0.25 are flagged as water. This threshold is slightly higher than the 0.2 ice fraction threshold used during the freeze-up and breakup detection process because I find

that a 0.25 ice fraction best matches with the USGS and WSC definitions of ice. On days with coincident observations, MODIS, USGS, and WSC ice flags are compared.

Additionally, freeze-up and breakup date results are validated against visual observations of ice on and ice off from the NWS. The NWS does not georeference the location of ice observations. Therefore, I manually georeference observations using site descriptions provided by the NWS. Locations with high uncertainty are not used for evaluation. The NWS ice dataset contains several different dates for ice on and ice off including first ice, freeze-up, safe for man, safe for vehicle, ice moved, breakup, first boat, unsafe for man, and unsafe for vehicle. For this analysis, only NWS 'breakup' and 'first ice' dates are used. I choose the NWS 'first ice' date because the MODIS freeze-up date is the date when the ice fraction goes above 0.2, which is more similar in definition to first ice than total river freeze-up. There are 21 unique locations and 102 total observations with both NWS 'first ice' and MODIS freeze-up observations. While the NWS 'last ice' date matches best with the MODIS definition of breakup, MODIS breakup dates are evaluated against NWS 'breakup' dates because there are approximately 4 times more observations of 'breakup' than 'last ice' since the year 2000. There 52 locations (612 total observations) that observe both NWS 'breakup' and MODIS breakup. MODIS ice on and off dates can occur on half days (eg. day of year 100.5), but NWS observations do not use fractional days. For comparison purposes, I use the floor of the MODIS breakup and freeze-up dates (eg. day of year 100.5 becomes day of year 100) when comparing to NWS data.

2.4 Trend analysis

I use the Regional Mann Kendall test (Helsel & Frans, 2006) and the seasonal Kendall slope estimator contained in the rkt package in R (Marchetto, 2017) to detect breakup date, freeze-up

date, and ice duration trends within each of the seven study regions. Reported p-values have been corrected for intra-block correlation (Libiseller & Grimvall, 2002).

To understand the interannual variability of river ice, I analyze the correlation of freeze-up and breakup dates to the PDO, the PNA, the EPNP, and the SOI. Breakup and freeze-up dates are also compared to regional monthly sea ice area measurements from the Bering Sea, the Chukchi Sea, and the Beaufort Sea. For each of the seven study regions, I first calculate the yearly median freeze-up and breakup days of the ice year. Next, Pearson's correlation coefficient (Pearson, 1896), *r*, is evaluated between the timeseries of regional median freeze-up dates and the mean teleconnection indices and sea ice areas from March-April-May (MAM) earlier in the calendar year, June-July-August (JJA), and September-October-November (SON). For spring breakup, I assess the teleconnection and sea ice correlations from the previous calendar year's SON, December-January-February (DJF), and the concurrent year's MAM. While Pearson's correlation is most commonly used for studying the relationship between teleconnections and river ice, Spearman's correlation coefficient results (ρ; Spearman, 1904), which tests for monotonic correlations, are included in **Appendix Figure 1** and **Appendix Figure 2**.

3. Results

3.1 Breakup and freeze-up patterns within individual rivers

This paper presents the first large-scale detection of ice freeze-up and breakup dates on all rivers wider than 150 m in Alaska and the Canadian portion of the Yukon River Basin (**Figure 3**). For six example rivers, the Yukon, the Koyukuk, the Porcupine, the Tanana, the Susitna, and the Colville, I show patterns of breakup and freeze-up progression through river systems, and how that progression changes from year to year (**Figure 4** & **Figure 5**). Breakup on the

Porcupine and the Susitna rivers is earlier near the mouth and progresses upstream (**Figure 4c** & **Figure 4e**). Yukon breakup progresses from upstream to downstream, except for reaches near the mouth of the river, which break up earlier (**Figure 4a**). For all rivers, spatial patterns of relatively early and relatively late breakup are similar each year. In contrast, spatial patterns of freeze-up are less spatially consistent through time. Spikes in freeze-up dates ~2000 km upstream on the Yukon River, ~290 km upstream on the Porcupine River, along the Tanana River, and near the mouth of the Colville River are likely caused by improperly filtered topographic and cloud shadows or freeze-up events that occurred during low light conditions.

3.2 Reach-specific evaluation of daily ice flags, breakup dates, and freeze-up dates

Evaluation of MODIS-derived ice flags against USGS and WSC discharge flags on individual reaches suggest that this method is quite accurate. I observe an overall accuracy of 0.97 and a kappa statistic of 0.93 when comparing MODIS ice flags to WSC 'B' flags, and an overall accuracy of .91 and a kappa statistic of 0.82 when compared to USGS 'e' flags. The months when breakup (April through June) and freeze-up (October and November) occur have the highest percentage of incorrect MODIS ice flags (**Table 1**). However, this pattern may be due in part to differences in ice flag definitions between MODIS flags, USGS flags, and WSC flags, which have the most substantial influence during transitional ice periods. The USGS and WSC flag discharge observations when the discharge-stage relationship at a gage is affected by ice, whether because of shore ice, bedfast ice, or total ice cover. This distinction is based on imagery, water temperature, air temperature, and the stage record itself (River Ice Processes, 2017). The USGS 'e' flag is also occasionally used when the stage-discharge relationship is influenced by factors other than ice. The 'e' flag is used during the summer, for example, during periods of flooding. Alternatively, WSC's 'B' flag is exclusively associated with ice presence.

Because WSC's 'B' flag is ice-specific, it makes sense that MODIS accuracy is higher when compared to WSC flags than to USGS flags.

I also evaluate breakup and freeze-up dates on individual reaches against NWS observations of 'first ice' dates and 'breakup' dates. When compared to NWS 'breakup' dates, MODIS breakup has a mean absolute error (MAE) of 4.17 days, a root-mean-square error (RMSE) of 6.29 days, and a mean bias error (MBE) of -2.85 days. For freeze-up, MAE is 10.46 days, RMSE is 22.44 days, and MBE is 6.60 days. However, two observations with large errors (> 75 days) caused by failures of the low light filter inflate MODIS freeze-up accuracy metrics. These observations are easily visually identifiable and will be removable with slight algorithm adjustments. The freeze-up error metrics excluding these outliers are 7.87 days (MAE), 11.03 days (RMSE) and 3.93 days (MBE).

3.3 Regional trends and correlations

Results show that breakup dates, freeze-up dates, and total ice duration vary regionally (**Figure 6**). Rivers on the North Slope of Alaska freeze a median of 17.5 days earlier and break up a median of 9.5 days later than the West Central region, the region with the next longest ice duration. Compared to the Southeast, North Slope rivers freeze up a median of 29.5 days earlier and break up a median of 28 days later, leading to a total ice duration of almost two months longer on the North Slope. Intraregional variability in freeze-up dates (calculated as the standard deviation of all freeze-up observations within a region) decreases from 38.5 days and 26.3 days, respectively, in the Southeast and Southwest regions to 9.9 and 22.5 days in the North Slope and West Central regions. In terms of breakup, intraregional variability is lowest within the North Slope (10.6 days), SW Yukon (10.0 days), and West Central (8.9 days) regions, and highest in the Southeast (18.9 days) and Southwest (22.7 days) regions.

Despite differences in the magnitude of breakup and freeze-up days of the year between regions, yearly median breakup and freeze-up dates among regions are often correlated, suggesting common drivers of ice on/off (**Table 2**). Breakup timing in the SE Yukon, Central Yukon, and SW Yukon regions are all strongly correlated to each other (r = 0.70-0.79), as are the Southwest and Southeast regions (r = 0.71). Breakup timing in the three Yukon regions is also moderately to strongly correlated to the Southwest of Alaska (r = 0.68-0.87), but only breakup in the SE Yukon region is strongly correlated to breakup in the Southeast region (r = 0.71). The North Slope is the least correlated to other regions, with only a more moderate correlation to the other western ocean-bordering regions (West Central, r = 0.62 and SW Yukon, r = 0.51) during breakup and no statistically significant correlations during freeze-up. Across all other regions, freeze-up date correlations are almost always weaker than breakup date correlations. The strongest freeze-up correlations (r = 0.74-0.83) are found between the regions in southwest and central Alaska (Southwest, SW Yukon, and Central Yukon). Freeze-up timing in the Southeast and SE Yukon are also correlated (r = 0.67). Ice timing in the West Central region is correlated to breakup in all regions as well as freeze-up in all regions except the North Slope.

The North Slope and West Central are the only two regions with statistically significant trends in breakup dates (-0.67 days/year at 95% confidence and -0.63 days/year at 90% confidence). West Central is the only region that shows a statistically significant trend in total ice duration (-1.10 days/year at 90% confidence). No regions have significant freeze-up date trends. While most of the regional trends are not statistically significant, statistically insignificant trends are all towards earlier breakup, later freeze-up, and shorter total ice duration (**Table 3**). Statistically significant long-term trends may be challenging to detect in this analysis because the

study period of eighteen years is too short and because interannual variability is high, particularly outside of the North Slope.

One of the potential sources of this interannual variability in freeze-up and breakup dates is the influence of climatological teleconnections that impact temperatures, storm paths, and precipitation over Alaska and Canada (Bonsal & Prowse, 2003; Bieniek et al., 2012). Both PDO and SOI indices in SON are moderately to strongly negatively correlated to the following spring's breakup dates in southern Alaskan regions (PDO: r = -0.59 to -0.77; SOI: r = 0.52 to 0.64), suggesting that high fall PDO values and low fall SOI values may be predictive of earlier regional breakup the following spring. EPNP indices and PNA indices are only correlated to breakup in DJF (PNA) and MAM (EPNP and PNA), and only within one (EPNP in MAM; PNA in DJF) or two (PNA in MAM) regions (**Figure 7**). Breakup and freeze-up dates on the North Slope are also not correlated to any of the studied teleconnections except for a moderate correlation between breakup dates and the EPNP during the spring (r = -0.55), where higher EPNP indices are associated with earlier breakup.

Freeze-up dates are much less frequently correlated to studied teleconnection indices (**Figure 8**). During freeze-up, the EPNP in the preceding MAM is significantly moderately correlated to fall freeze-up dates in the Southwest (r = 0.60), Southeast (r = 0.57), and SW Yukon (r = 0.56) regions. High spring EPNP indices predict later fall freeze-up. Positive PDO values and negative SOI values in SON are also associated with later fall freeze-up dates in the Southwest (PDO: r = 0.61; SOI: r = -0.48) and SW Yukon (PDO: r = 0.59; SOI: r = -0.47) regions.

Another potential source of interannual variability in breakup and freeze-up is variability in sea ice area, which can influence precipitation over North America (Sewall, 2005; Kopec et al., 2016). Expectedly, sea ice area is most strongly correlated to breakup during the spring (MAM).

Bering Sea ice is moderately correlated to breakup dates in the Southwest (r = 0.60) and Southeast (r = 0.56) regions. Chukchi Sea ice area is correlated (r = 0.64 – 0.66) to all regions bordering the Alaskan west coast (Southwest, SW Yukon, West Central, and North Slope). While these results suggest that correlation may be related to proximity between land regions and oceanic regions, Beaufort Sea ice area is moderately to strongly correlated to breakup dates in all Alaskan regions (r = 0.47 – 0.73). The correlation of freeze-up dates to sea ice area is much more localized, where freeze-up in the Southwest region significantly correlates only to Bering Sea ice area (r = -0.54), and Beaufort Sea ice area only significantly correlates to freeze-up on the North Slope (r = -0.48). Statistically significant correlations between sea ice and breakup dates are always positive, indicating an association between larger ice area and later ice breakup. Statistically significant correlations between sea ice area and freeze-up timing are always negative, indicating an association between larger ice area and earlier freeze-up dates.

4. Discussion

This study represents the first quantification of breakup and freeze-up dates on rivers narrower than 500 m and is the first large-scale detection of river ice freeze-up from space. Patterns in breakup and freeze-up timing can be used to understand and quantify drivers of spatial and temporal river ice variability.

4.1 Local breakup and freeze-up drivers

Analysis of river profiles allows the investigation of drivers in ice timing variability within individual rivers. For example, both the Susitna and Porcupine flow south from mountainous regions to lower elevations. This is likely why breakup in both rivers progresses from the mouth of the river towards upstream reaches, and why freeze-up progresses from the upstream reaches towards the mouth (**Figure 4c** & **Figure 4e**; **Figure 5c** & **Figure 5e**). This pattern contrasts with

many large Arctic rivers that are north-flowing, such as the Lena, the Mackenzie, the Ob', and the Yenisey (Pavelsky & Smith, 2004; Cooley & Pavelsky, 2016). The Koyukuk is also a south-flowing river, but patterns of breakup are much less linear than on the Porcupine and Susitna. Certain rapid changes in breakup on the Koyukuk seem to correlate with sharp changes in elevation (~475 km upstream and ~630 km upstream; **Figure 4c**). Further analysis of channel geomorphology, river curvature, slope, and air temperature may also provide insights on the drivers of local patterns of Koyukuk ice breakup.

Ice phenology on the Yukon mainstem is influenced by tributaries; breakup occurs earlier and freeze-up later near the confluence with the Tanana River, a tributary from the south. However, neither breakup nor freeze-up dates are influenced by confluences with rivers flowing in from the north such as the Porcupine and the Koyukuk (**Figure 4a**; **Figure 5a**). Breakup dates on the Yukon are particularly interesting because breakup near the mouth is variable, which, upon visual inspection of MODIS imagery, seems to correspond to shore-fast sea ice presence at the mouth of the river. The north to south flowing portion of the Yukon (~250-475 km upstream on **Figure 4a**) breaks up earlier downstream and later upstream, suggesting latitudinal drivers of breakup timing. The rest of the Yukon breaks up earliest in the upstream reaches near Eagle, Alaska, which is relatively southern, and then progresses on a path northward, then back southward, and always downstream. The spatial similarity between relatively early and relatively late breakup reaches year to year within each river suggests that the control of breakup variability between years is predominately regional in nature.

Overall, patterns in freeze-up are much less spatially consistent through time. There are also more reaches during freeze-up whose observations were removed due to high uncertainty. This is caused both by more frequent clouds during the freeze-up period and by freeze-ups that occurs

during low-light periods, especially in areas of high topographic variation, such as the middle reaches of the Susitna River (**Figure 5e**). Spikes in freeze-up dates on the Tanana river in 2003 are caused by reaches that either do not freeze prior to onset of low-light conditions or because clouds or cloud shadows obscure the entire freeze-up process before low-light conditions take effect. Instead of the actual freeze-up, the algorithm detects the increase in reflectance towards the end of low light conditions, the observations of which are not properly removed during data filtering.

4.2 Regional trends and correlations

While long-term trends explain some of the variation in breakup and freeze-up dates, variability over the period studied here is predominately interannual. Positive PDO anomalies and negative SOI anomalies correlate to earlier breakup in southern and central Alaska even up to nine months prior to breakup events, indicating regional predictability. This predictability, if quantified further, could be useful to Alaskan residents and industry who rely on ice roads for transportation and shipping as well as for hunting and trapping (Stephenson et al., 2011) and may have implications for ice jam flood risk predictability due to the correlation between teleconnections, air temperature, and precipitation (Hartmann & Wendler, 2005).

The relationship between spring PDO and spring breakup timing has previously been noted in Western Canada, Northwestern Canada, and Eastern Siberia (Pavelsky & Smith, 2004; Bonsal et al., 2006) as has the relationship between earlier breakup and El Niño conditions (which correspond to negative SOI anomalies) for several locations in Alaska (Bieniek et al., 2011) and Western Canada (Bonsal et al., 2006). Bieniek et al. (2011) suggests that winter El Niño conditions lead to fewer storms in the Gulf of Alaska, fewer clouds, and warmer air temperatures which causes earlier river ice breakup. The PDO is not correlated to breakup on the North Slope,

likely because North Slope air temperature is not significantly correlated to the PDO (Bieniek et al., 2012).

Bienek et al. (2012) found that EPNP indices during the months of DJF and MAM have the strongest correlation to air temperature on the North Slope of Alaska. Consequently, the only statistically significant correlation between a teleconnection index and North Slope breakup timing is to the EPNP during MAM. MAM EPNP is also moderately correlated to fall freeze-up dates in the southern regions of Alaska, which is unexpected because EPNP is rarely correlated to air temperature outside of the North Slope (Bieniek et al., 2012).

I also observe a positive correlation between sea ice area in the Bering Sea during SON, DJF, and MAM, and southern Alaska breakup timing. This indicates that larger sea ice areas in the fall and winter are predictive of later river ice breakup timing in the following spring in southern Alaska. I see moderate positive correlations between breakup timing and Chukchi sea ice area in DJF, which increase in strength during the months of MAM along the entire west coast of Alaska. In MAM, there are statistically significant positive correlations between river ice breakup in all regions and ice area in the Beaufort Sea. This pattern of correlations could be related to sea-ice driven changes in precipitation, where more sea ice results in less Alaskan precipitation (Kopec et al., 2016; Sewall, 2005) which causes later breakup. However, this explanation is counter to analysis by Bieniek et al., (2011), who found that increases in precipitation cause later breakup in southern Alaska. More likely is that patterns controlling air temperature in Alaska and the North Pacific Ocean influence both sea ice and river ice breakup, hence the positive correlation between the two. For example, SOI is significantly correlated to both river ice breakup and sea ice area in the Bering Sea (Niebauer, 1988), where negative SOI anomalies 9-12 months in advance precede warmer air temperatures and smaller sea ice areas

(Niebauer, 1988). Alternatively, sea ice loss is thought to be a driver of increased air temperatures in Alaska (Serreze et al., 2007; Lawrence et al., 2008; Deser et al., 2010) as well as regional changes in precipitation amount and type (Deser et al., 2010). Increased air temperatures associated with predicted sea ice loss may cause future later freeze-ups and earlier breakups in Alaskan rivers. The future direction and magnitude of precipitation changes due to sea ice loss is not yet well constrained in Alaska (Deser et al., 2010).

4.3 Uncertainties

There are several potential sources of error in our observations. First, uncertainties in freeze-up and breakup date calculations caused by cloudy imagery (mean/median freeze-up uncertainty: ±8.4/3.5 days; mean/median breakup uncertainty: ±3.2/2 days; **Figure 9**) can propagate through to trend and correlation analysis. However, this error is reduced by analyzing data regionally as opposed to on a reach-by-reach basis. I also acknowledge the temporal limitations of studying climate patterns over an eighteen-year time period. In the future, correlations could be recalculated as more MODIS data becomes available. Similarities between Pearson's correlation coefficients (**Figure 7** & **Figure 8**) and Spearman's correlation coefficients (**Appendix Figure 1** & **Appendix Figure 2**), particularly between fall PDO and SOI indices and spring breakup dates, strengthens my confidence in these relationships.

Another potential source of error is the stationary water mask used to identify river-observing pixels, which does not account for the movement of Arctic rivers over the study period. The USGS and NASA recently released the MOD44W.006 water mask product, which is a yearly version of the product used in this study. However, water masks for 2016 and 2017 are not yet available on Google Earth Engine. Future analyses should incorporate this updated product as it becomes available. Lastly, in certain locations, freeze-up timing can be impacted by topographic

shadows not removed during the data filtering process. However, these errors are uncommon and are easily manually identifiable in the original MODIS imagery.

5. Conclusion

These results provide the first reach-scale detection of river ice freeze-up dates, breakup dates, and total ice duration on Alaskan river reaches wider than 150 m. Preliminary analyses of river profiles demonstrate the utility of this dataset to assist in identifying localized drivers of breakup and freeze-up timing. While long-timescale trends in freeze-up and breakup dates are rarely detected, it is unclear if the lack of trends is caused by river ice processes that are not changing in response to climate warming or if the timescale of this study is too short to capture these patterns. However, south of the Brooks Range, much of the interannual variability in ice timing is explained by teleconnections, particularly the PDO and the SOI, whose fall indices may be predictive of regional spring breakup timing. Correlations between freeze-up timing and teleconnections are generally weaker and less persistent throughout the entire state of Alaska. Future analyses should use this dataset in conjunction with geomorphological data to better constrain localized drivers of ice timing and should work to quantify the predictive power of fall teleconnections for regional spring breakup. Ice detection methods presented in this paper are expandable to pan-Arctic rivers, and such analysis would improve understanding of patterns and drivers of river ice in a changing Arctic environment.

FIGURES

Figure 1. Map of Alaskan river reaches with median widths wider than 150 m. USGS gage stations available for validation are shown in red. The number of reaches per study region in which ice timing was able to be analyzed is also listed.

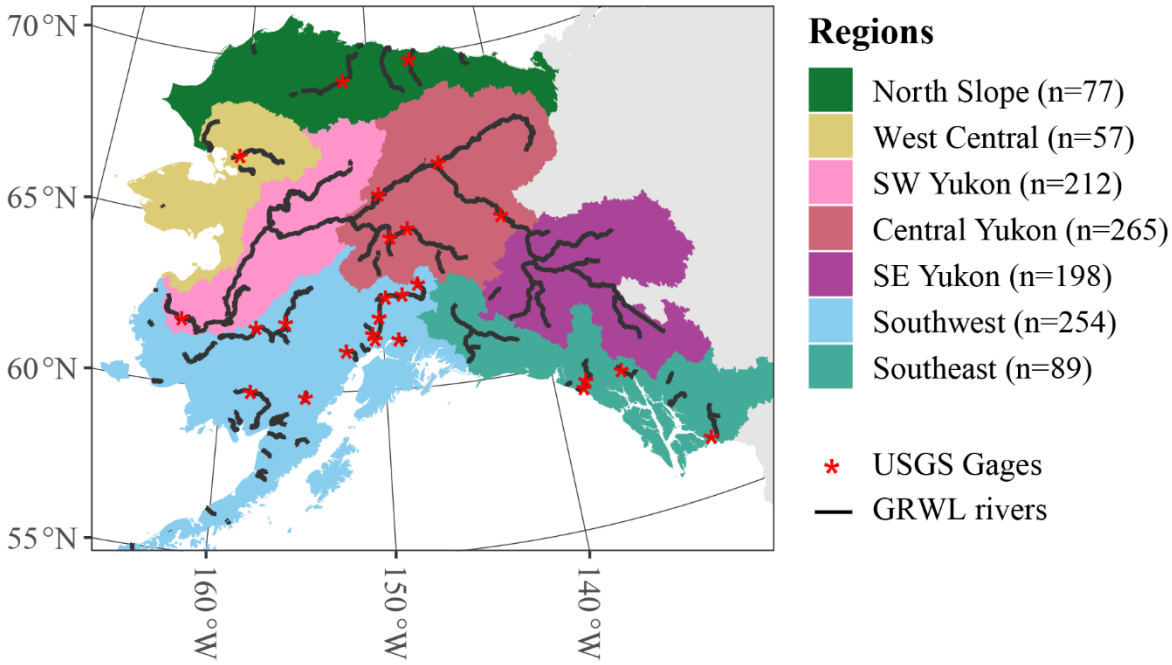

Figure 2: a. A demonstration of cumulative cost mapping using GRWL river centerlines (red) to distinguish river pixels (blue) from miscellaneous water pixels (green) in the MOD44W.005 water mask. The bottom right corner of image is ~10 km downstream from Nenana, AK. The arrow shows the direction of flow of the Tanana River. The black box contains the reach used in b. and c. **b.** An example density plot of red band reflectance values for January through July 2000-2017 from the reach highlighted in a. The dashed black line represents the surface reflectance threshold used to classify pixels in that reach as either water or ice. **c.** An example ice fraction time series for the same reach in ice year 2016, with spikes and pits shown in red, the freeze-up date in teal, and the breakup date in pink. Uncertainties in ice timing dates due to missing cloudy data are shown by black horizontal error bars. The low-light period is highlighted in gray.

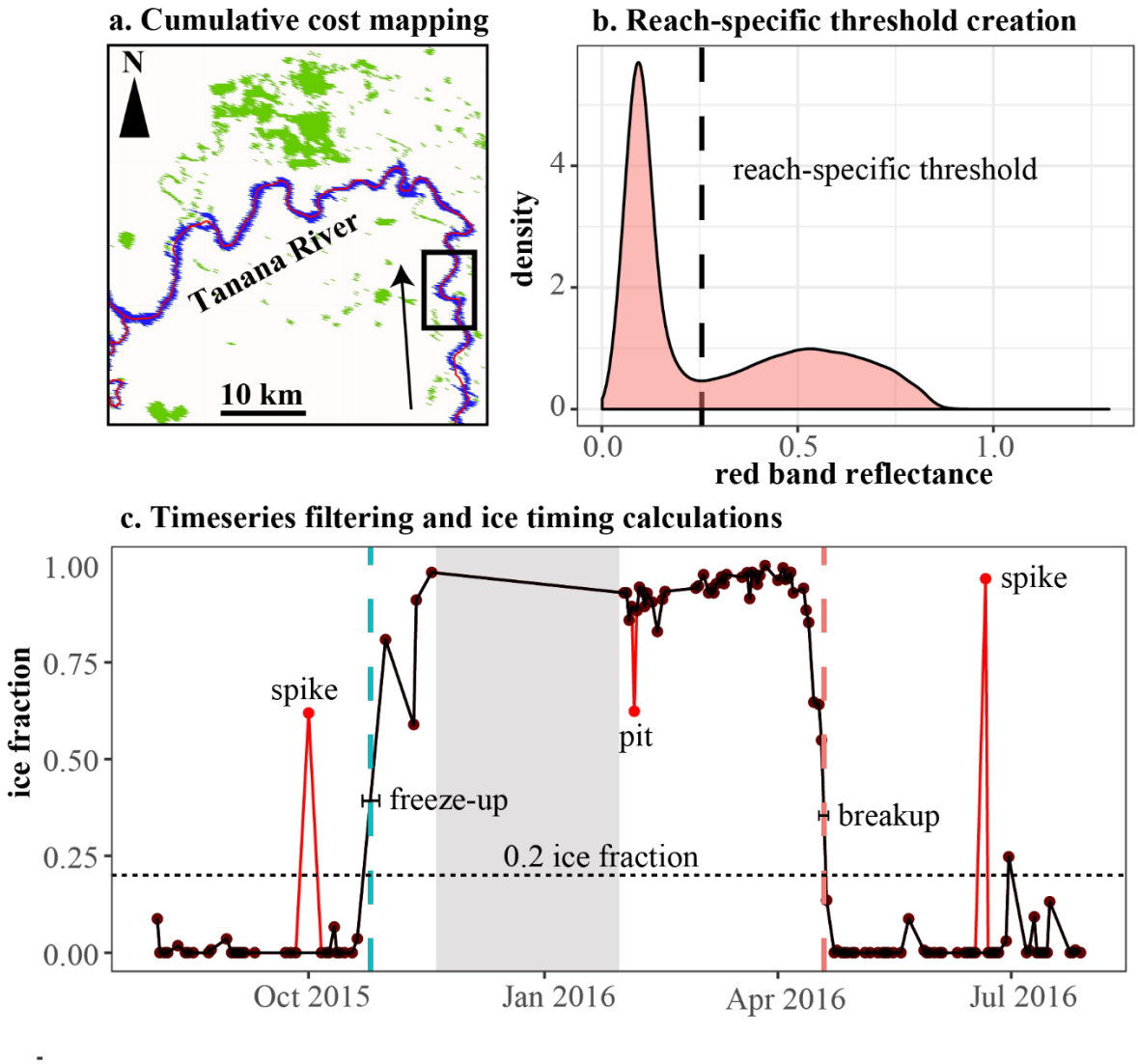

Figure 3: a. Median freeze-up day of the ice year. **b.** Median breakup day of the ice year.

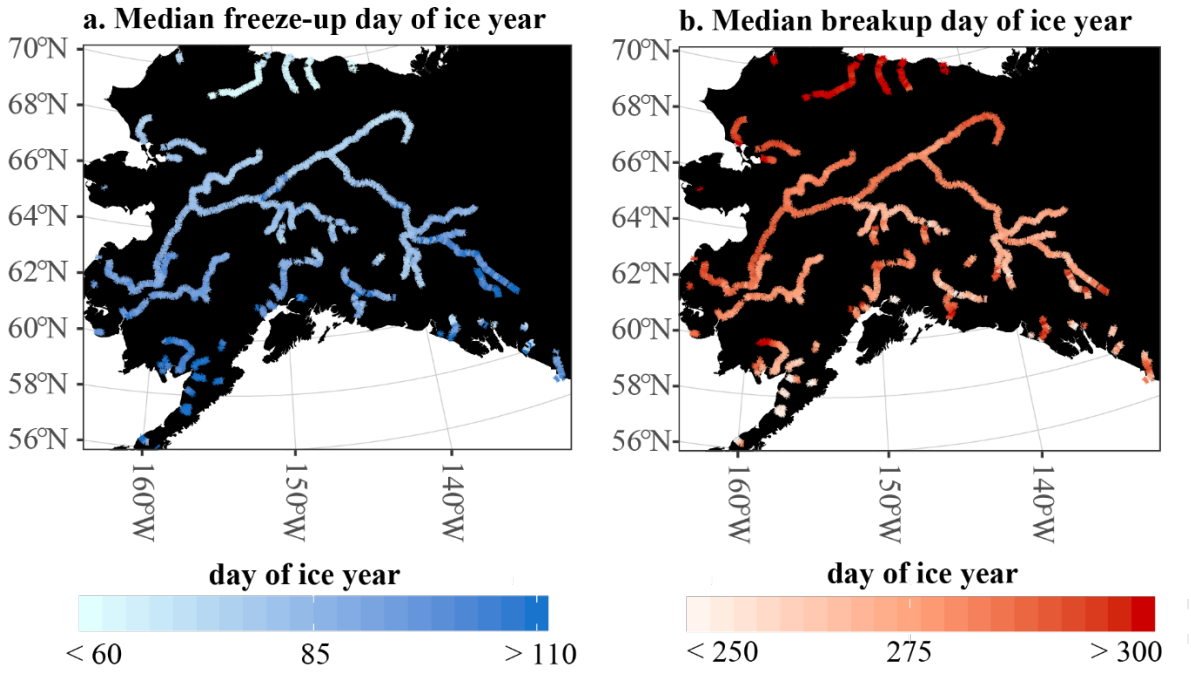

Figure 4: a-f. Ice breakup day of the ice year (DOY) for the (a) Yukon, (b) Koyukuk, (c) Porcupine, (d) Tanana, (e) Susitna, and (f) Colville rivers. Gray areas represent reaches with topographic-shadow risk where the standard deviation of topography within 2 km of the centerline is greater than 100 m. On each plot, 0 km refers to **a.** 10 km downstream of Mountain Village Airport, AK. **b.** The mouth of the Koyukuk River. **c.** The mouth of the Porcupine River. **d.** The mouth of the Tanana river. **e.** ~10 km downstream of the Yetna River confluence with the Susitna River. **f.** ~40 km upstream from the mouth of the Colville River.

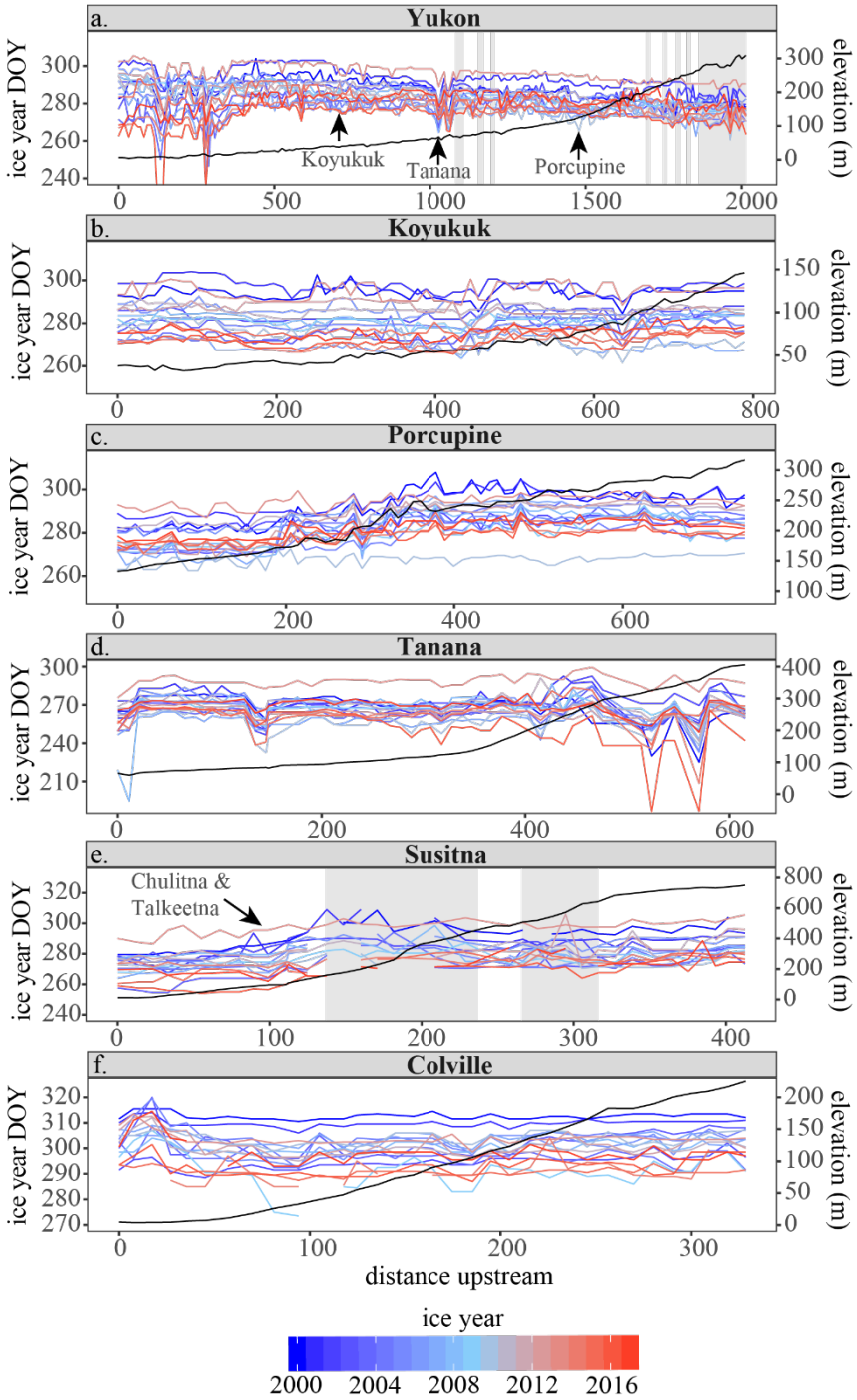

Figure 5: a-f. Same as Figure 4 except for freeze-up day of the ice year (DOY).

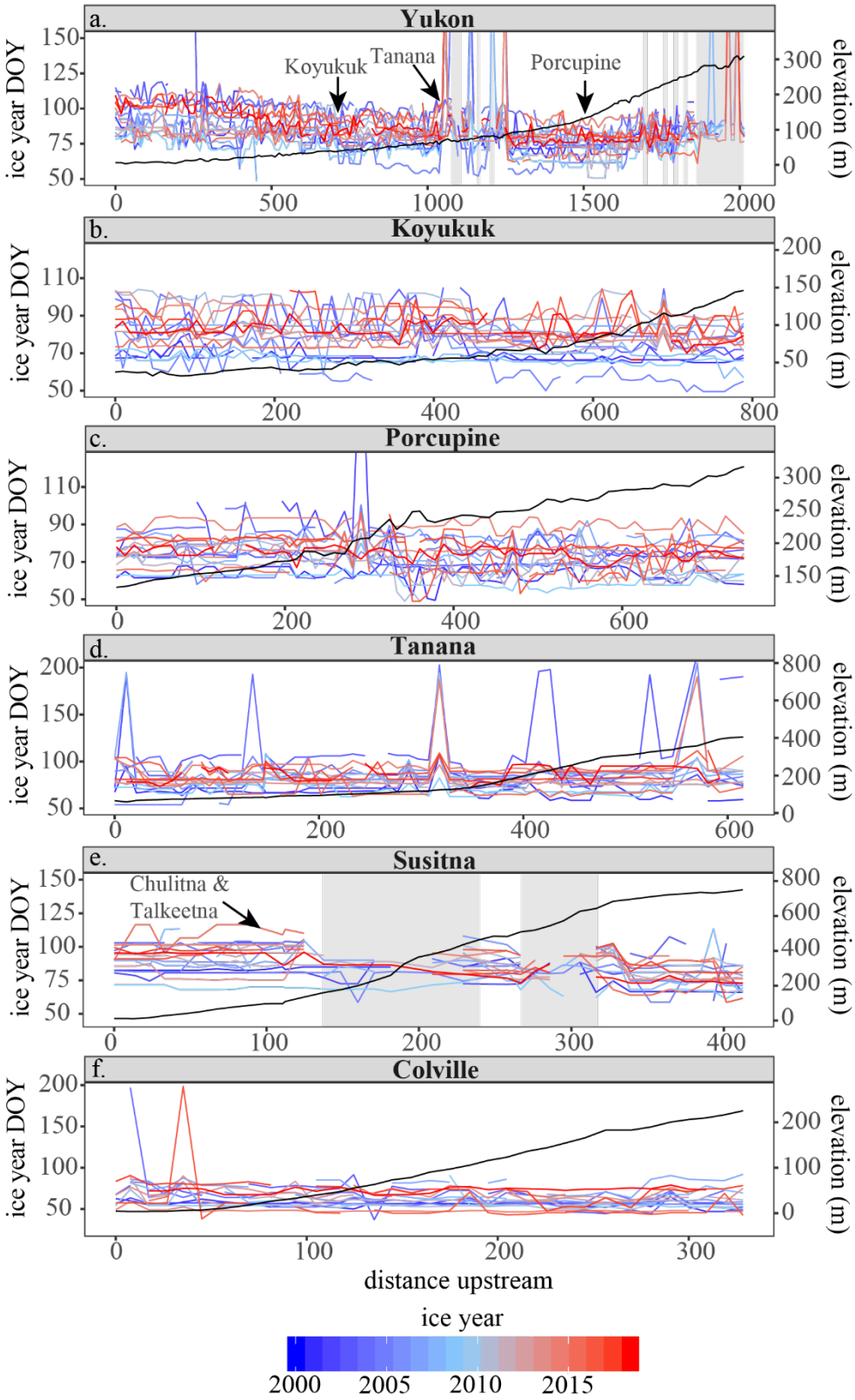

Figure 6: a. Regional timeseries of median breakup and freeze-up days of the ice year. **b.** Regional median total ice duration.

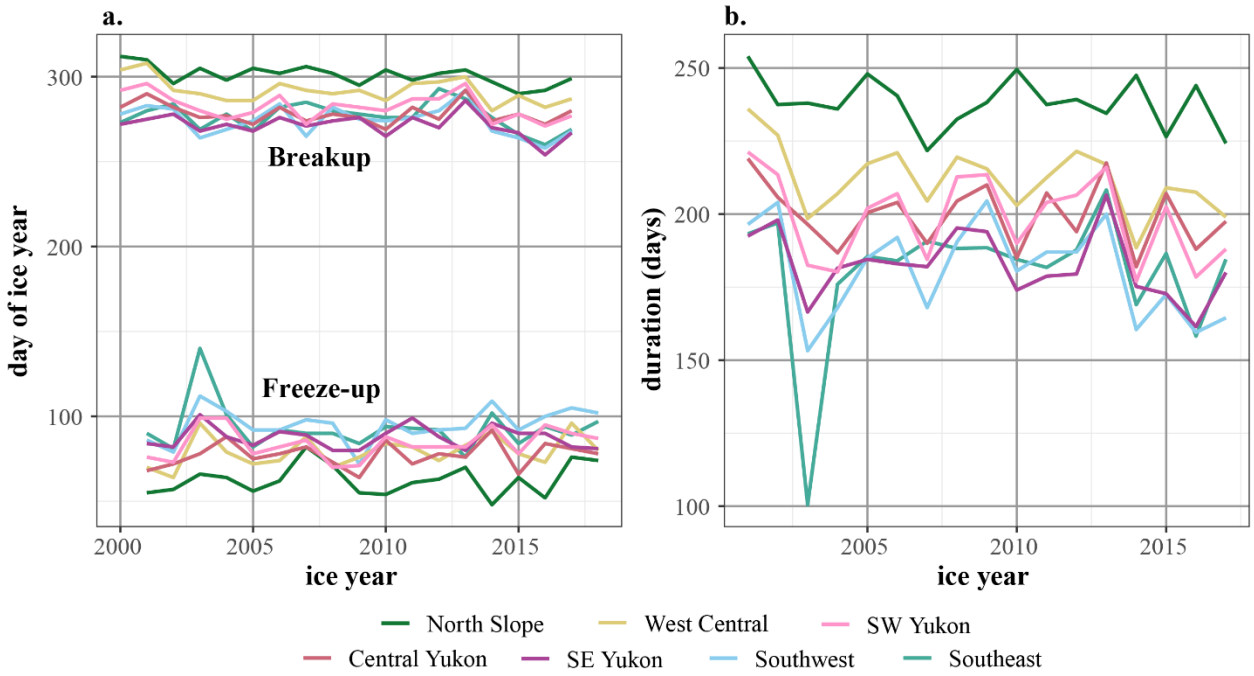

Figure 7: Pearson's correlation coefficients between regional median breakup dates, mean teleconnection indices, and regional mean sea ice areas during SON, DJF, and MAM. Statistically significant (p-value <0.05) correlations are shown with a black outline.

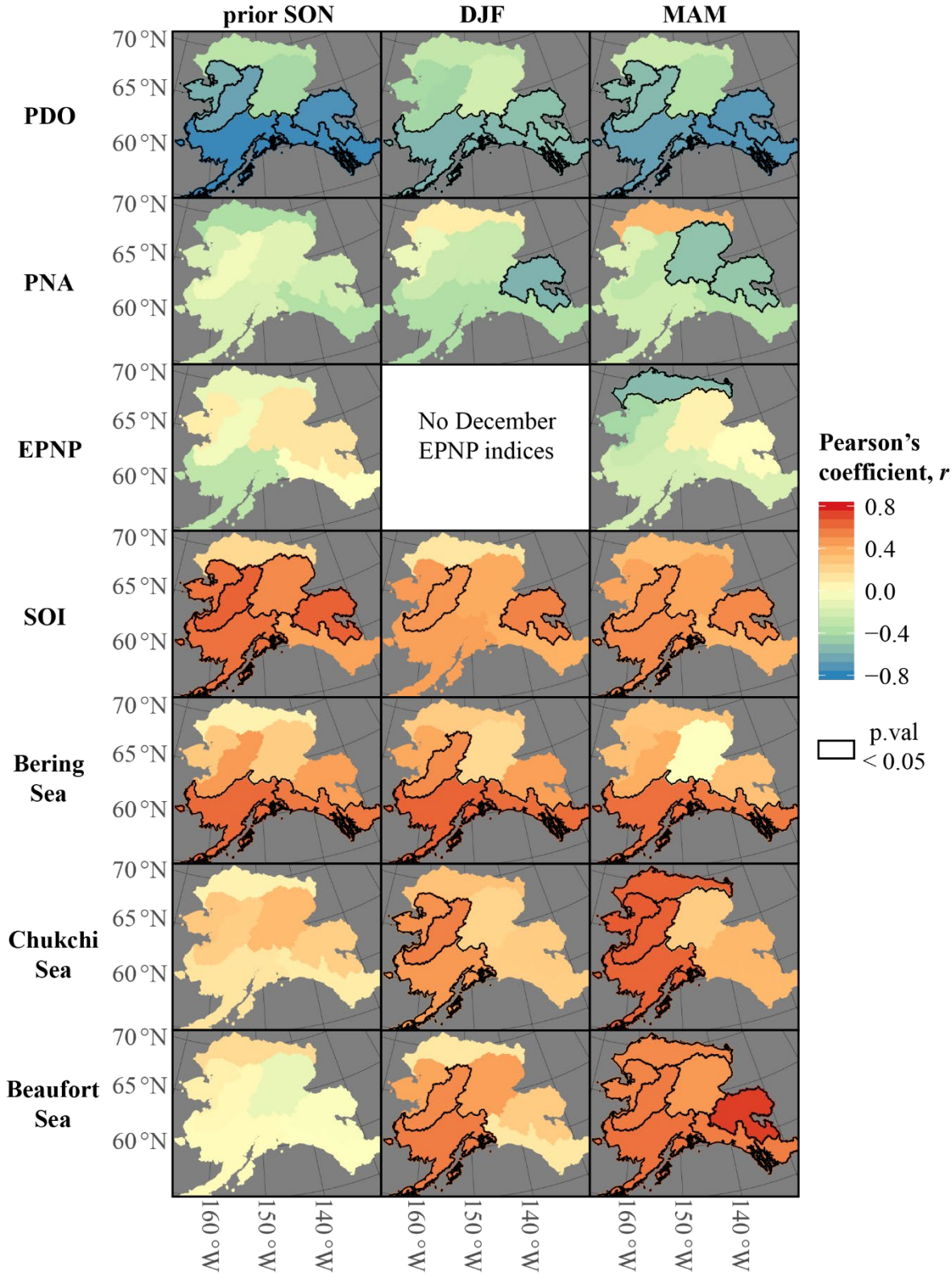

Figure 8: Pearson's correlation coefficients between regional median freeze-up dates, mean teleconnection indices, and regional mean sea ice areas during MMA, JJA, and SON. Statistically significant (p-value <0.05) correlations are shown with a black outline.

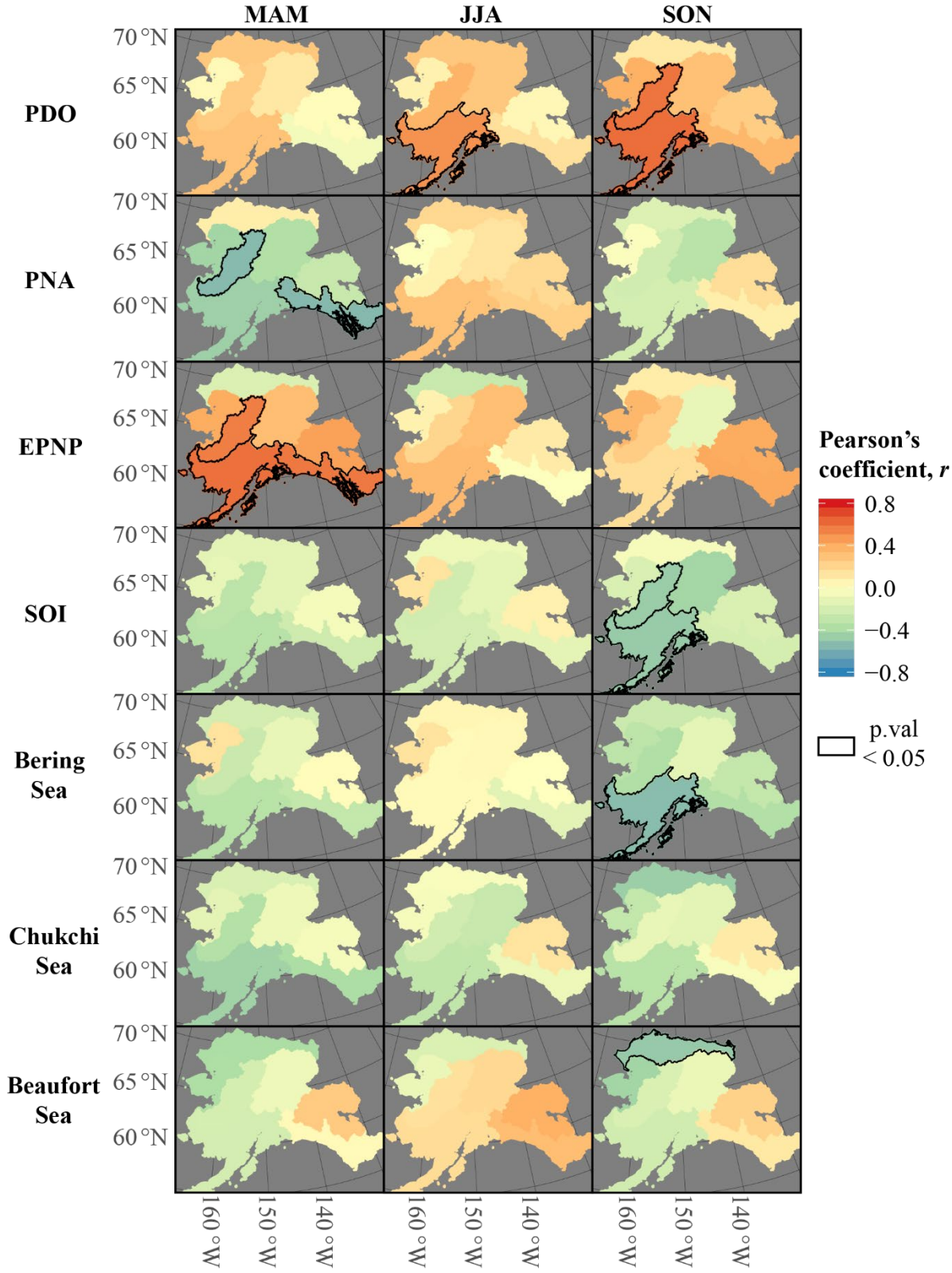

Figure 9: Median uncertainty caused by missing cloudy data in **a.** freeze-up and **b.** breakup.

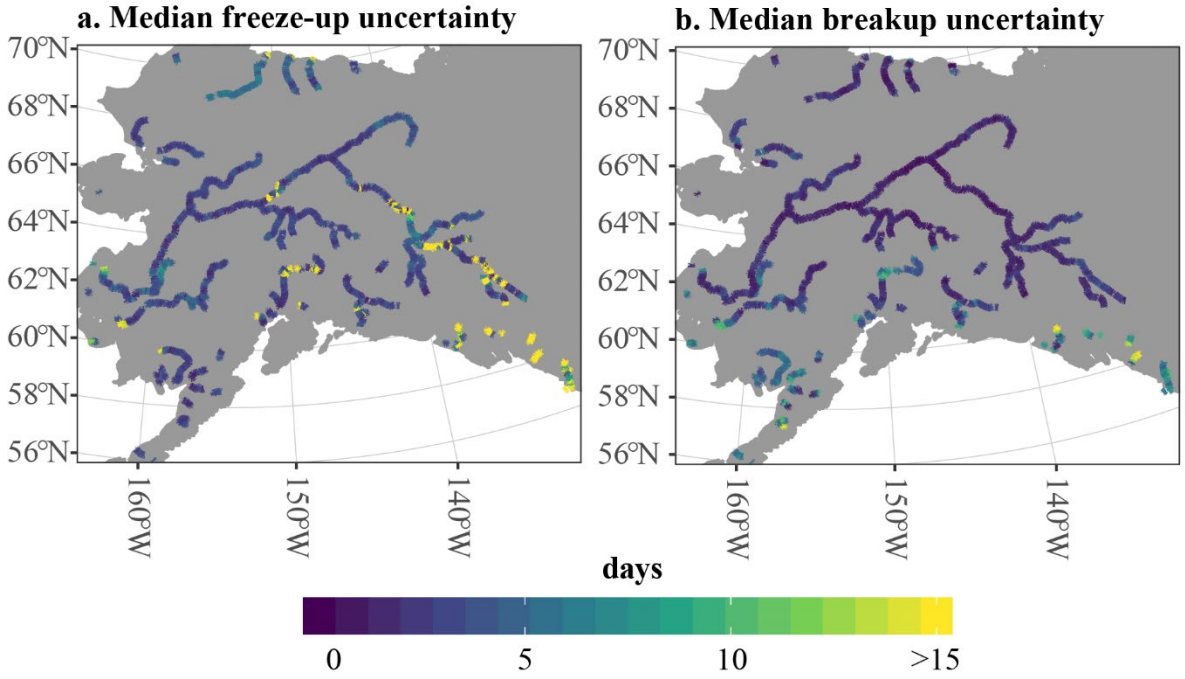

TABLES

Table 1: Total number of coincident WSC/USGS and MODIS observations and the percentage of observations where MODIS ice flags disagree with WSC/USGS ice flags.

	WSC		USGS	
	No. of coincident obs.	**% incorrect**	**No. of coincident obs.**	**% incorrect**
January	5896	1.5	116	1.7
February	8033	0.4	1847	0.9
March	10154	1.6	3165	0.7
April	12151	8.0	2939	11.8
May	13991	7.3	2999	24.1
June	15849	2.6	3157	5.8
July	17881	0.3	2753	4.5
August	15924	0.1	2510	2.4
September	13933	0.1	2352	3.4
October	9520	4.1	1907	19.8
November	7190	13.5	1155	18.7
December	5908	5.8	55	0

Table 2: **a.** Pearson's correlation coefficients between median breakup timeseries for each region. **b.** same as a. but for freeze-up dates.

a. Breakup Correlation Coefficients

	North Slope	**West Central**	**SW Yukon**	**Central Yukon**	**SE Yukon**	**Southwest**	**Southeast**
North Slope							
West Central	0.62**						
SW Yukon	0.51**	0.89**					
Central Yukon	0.29	0.76**	0.79**				
SE Yukon	0.27	0.60**	0.70**	0.73**			
Southwest	0.43*	.67**	0.87**	0.68**	0.82**		
Southeast	0.33	0.49**	0.49**	0.35	0.71**	0.71**	

b. Freeze-up Correlation Coefficients

	North Slope	**West Central**	**SW Yukon**	**Central Yukon**	**SE Yukon**	**Southwest**	**Southeast**
North Slope							
West Central	0.35						
SW Yukon	0.02	0.65**					
Central Yukon	-0.05	0.45*	0.80**				
SE Yukon	-0.26	0.45*	0.56*	0.31			
Southwest	0.26	0.68**	0.83**	0.74**	0.43*		
Southeast	0	0.51**	0.65**	0.33	0.67**	0.64**	

Pearson's *r*: * 0.1 significance, ** 0.05 significance

Table 3: Kendall's **τ** and Sen's seasonal slope estimator for freeze-up, breakup, and total ice duration within each of the study regions.

	Freeze-up		**Breakup**		**Ice duration**	
	Kendall's τ	**Slope (days/year)**	**Kendall's τ**	**Slope (days/year)**	**Kendall's τ**	**Slope days/year**
North Slope	0.13	0.42	-0.32**	-0.67	-0.17	-0.67
W Central	0.18	0.50	-0.28*	-0.63	-0.28*	-1.10
SE Yukon	0.04	0.08	-0.20	-0.43	-0.18	-0.77
Central Yukon	0.11	0.30	-0.16	-0.31	-0.10	-0.42
SW Yukon	0.17	0.50	-0.22	-0.50	-0.19	-0.93
SW Alaska	0.12	0.50	-0.17	-0.50	-0.16	-1.00
SE Alaska	0.02	0.07	-0.15	-0.46	-0.09	-0.50

APPENDIX: SPEARMAN'S CORRELATION

Appendix Figure 1: Spearman's correlation coefficients between regional median breakup dates, mean teleconnection indices, and regional mean sea ice areas during SON, DJF, and MAM. Statistically significant (p-value <0.05) correlations are shown with a black outline.

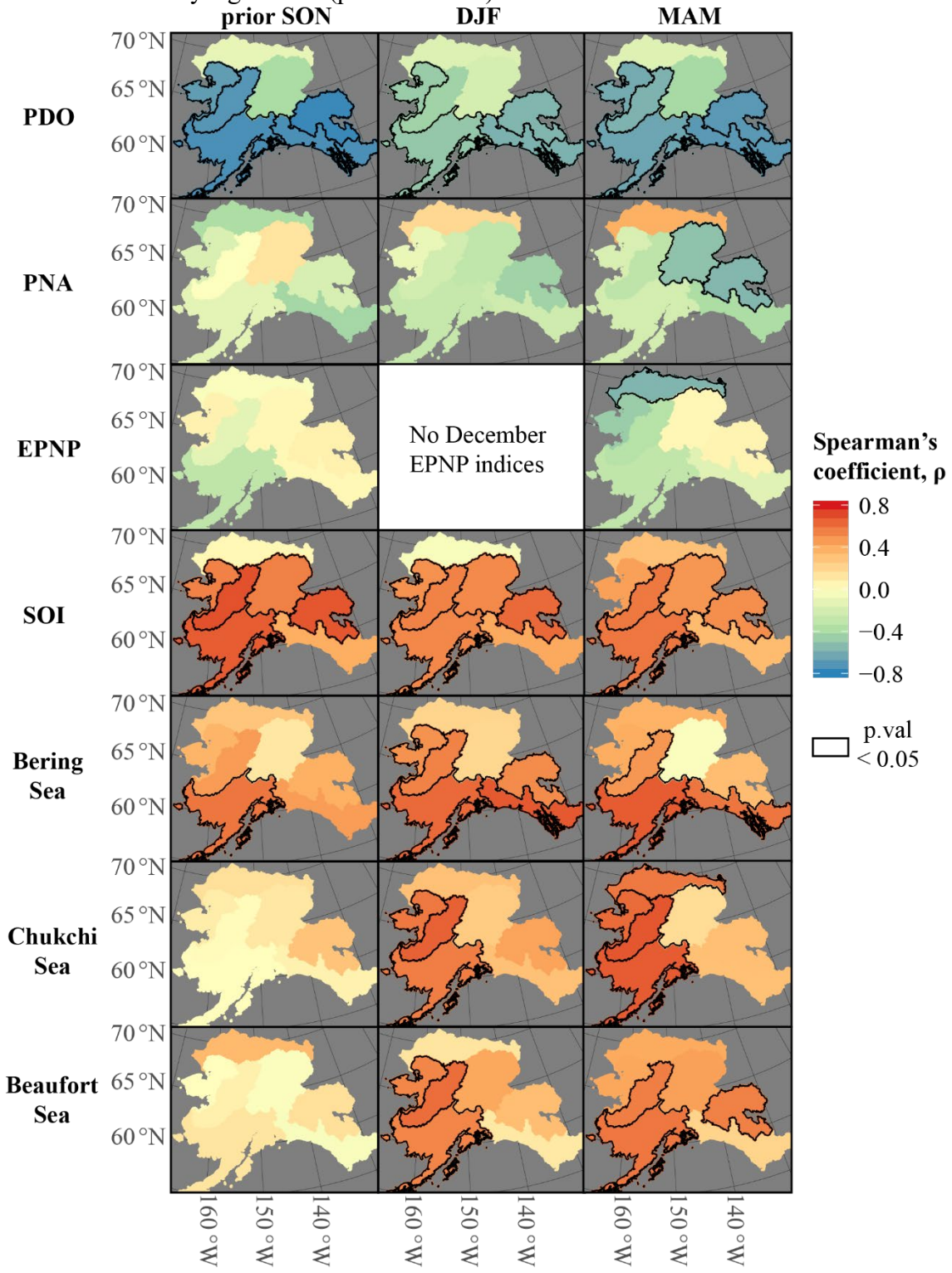

Appendix Figure 2: Spearman's correlation coefficients between regional median freeze-up dates, mean teleconnection indices, and regional mean sea ice areas during MAM, JJA, and SON. Statistically significant (p-value <0.05) correlations are shown with a black outline.

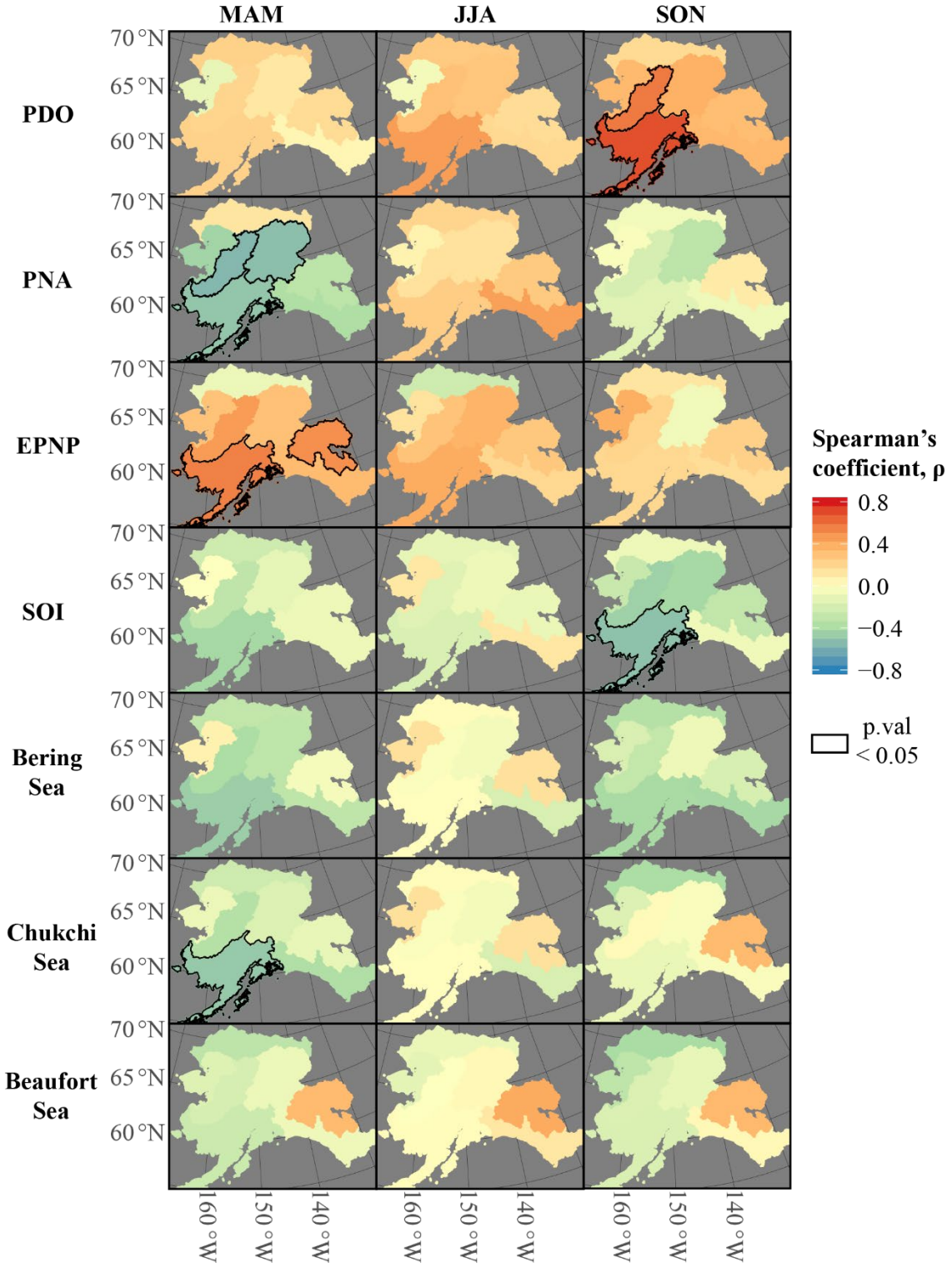

REFERENCES

Allen, G. and Pavelsky, T. (2018). Global extent of rivers and streams. *Science,* 361, 585-588. https://doi.org/10.1126/science.aat0636

Arp, C.D., Jones, B.M., & Grosse, G. (2013). Recent lake ice-out phenology within and among lake districts of Alaska, U.S.A. *Limnology & Oceanography,* 58(6), 2013-2028. https://doi.org/10.4319/lo.2013.58.6.2013

Barnston, A.G., & Livezey, R.E. (1987). Classification, seasonality and persistence of low-frequency atmospheric circulation patterns. *Monthly Weather Review,* 115, 1083-1126. https://doi.org/10.1175/1520-0493(1987)115%3C1083:CSAPOL%3E2.0.CO;2

Bell, G.D., & Janowiak, J.E. (1995). Atmospheric Circulation Associated With the Midwest Floods of 1993. *Bulletin of the American Meteorological Society,* 76, 681-696. https://doi.org/10.1175/1520-0477(1995)076%3C0681:ACAWTM%3E2.0.CO;2

Beltaos, S., & Prowse, T. (2009). River-ice hydrology in a shrinking cryosphere. *Hydrological Processes,* 23, 122-144. https://doi.org/10.1002/hyp.7165

Bennett, K.E., & Prowse, T.D. (2010). Northern Hemisphere geography of ice-covered rivers. *Hydrological Processes,* 24, 235-240. https://doi.org/ 10.1002/hyp.7561

Benson, B., Magnuson, J., & Sharma, S. (2000). *Global Lake and River Ice Phenology Database, Version 1*, https://nsidc.org/data/g01377?qt, National Snow and Ice Data Center, Boulder, Colorado.

Bieniek, P.A., Bhatt, U.S., Rundquist, L.A., Lindsey, S.D., Zhang, X., & Thoman, R.L. (2011). Large-Scale Climate Controls of Interior Alaska River Ice Breakup. *Journal of Climate,* 24, 286-297. https://doi.org/10.1175/2010JCLI3809.1

Bieniek, P.A., Bhatt, U.S., Thoman, R.L., Angeloff, H., Partain, J., Papineau, J., et al. (2012). Climate Divisions for Alaska Based on Objective Methods. *Journal of Applied Meteorology and Climatology,* 51, 1276-1298. https://doi.org/10.1175/JAMC-D-11-0168.1

Bonsal, B.R., Prowse, T.D., Duguay, C.R., & Lacroix, M.P. (2006). Impacts of large-scale teleconnections on freshwater-ice break/freeze-up dates over Canada. *Journal of Hydrology,* 330, 340-353. https://doi.org/10.1016/j.jhydrol.2006.03.022

Bonsal, B.R., & Prowse, T.D. (2003). Trends and Variability in Spring and Autumn 0°C-Isotherm Dates over Canada. *Climate Change,* 57, 341-358. https://doi.org/10.1023/A:1022810531237

Carroll, M.L., DiMiceli, C.M., Wooten, M.R., Hubbard, A.B., Sohlberg, R.A., Townshend, J.R.G. (2017). *MOD44W MODIS/Terra Land Water Mask Derived from MODIS and SRTM L3 Global 250m SIN Grid V006*. NASA EOSDIS Land Processes DAAC. https://doi.org/10.5067/MODIS/MOD44W.006

Carrol, M.L., Townshend, J.R., DiMiceli, C.M., Noojipady, P., & Sohlberg, R.A. (2009). A new global raster water mask at 250 m resolution. *International Journal of Digital Earth,* 2(4), 291-308. https://doi.org/10.1080/17538940902951401

Chaouch, N., Temimi, M., Romanov, P., Cabrera, R., McKillop, G., & Khanbilvardi, R. (2014). An automated algorithm for river ice monitoring over the Susquehanna River using the MODIS data. *Hydrological Processes,* 28, 62-73. http://doi.org/10.1002/hyp.9548

Chu, T., & Lindenschmidt, K. (2016). Integration of space-borne and air-borne data in monitoring river ice processes in the Slave River, Canada. *Remote Sensing of Environment,* 181, 65-81. http://dx.doi.org/10.1016/j.rse.2016.03.041

Colwell, J.E. (1974). Vegetation Canopy Reflectance. *Remote Sensing of Environment,* 3, 175-183.

Cooley, S., & Pavelsky, T. (2016). Spatial and temporal patterns in Arctic river ice breakup revealed by automated ice detection from MODIS imagery. *Remote Sensing of Environment,* 175, 310-322. http://dx.doi.org/10.1016/j.rse.2016.01.004

Deser, C., Tomas, R., Alexander, M., Lawrence, D. (2010). The Seasonal Atmospheric Response to Projected Arctic Sea Ice Loss in the Late Twenty-First Century. *Journal of Climate,* 23, 333-351. https://doi.org/10.1175/2009JCLI3053.1

Duguay, C.R., Prowse, T.D., Bonsal, B.R., Brown, R.D., Lacroix, M.P., & Ménard, P. (2006). Recent trends in Canadian lake ice cover. *Hydrological Processes,* 20, 781-801. https://doi.org/10.1002/hyp.6131

Fetterer, F., Knowles, K., Meier, W.N., Savoie, M., & Windnagel, A.K. (2017 to present, updated daily). *Sea Ice Index, Version 3.* Boulder, Colorado, USA. NSIDC: National Snow and Ice Data Center. https://doi.org/10.7265/N5K072F8

Gauthier, Y., Hardy, S., Gutiérrez, C., Padel, A., Gaudreau, J.P., Jasek, M., et al. (2015). *IceFRONT: Integration of radar and optical images for operational river freeze-up monitoring*. Paper Presented at 18th Workshop on the Hydraulics of Ice Covered Rivers, Quebec City, QC.

Global Modeling and Assimilation Office (GMAO). (2015). *MERRA-2 statD_2d_slv_Nx: 2d,Daily,Aggregated Statistics,Single-Level,Assimilation,Single-Level Diagnostics V5.12.4*, Greenbelt, MD, USA, Goddard Earth Sciences Data and Information Services Center (GES DISC), https://doi.org/10.5067/9SC1VNTWGWV3

Hartmann, B., & Wendler, G. (2005). The Significance of the 1976 Pacific Climate Shift in the Climatology of Alaska. *Journal of Climate,* 18, 4824-4839. https://doi.org/10.1175/JCLI3532.1

Helsel, D.R., & Frans, L.M. (2006). The Regional Kendall test for trend. *Environmental Science and Technology,* 40, 4066-4073. https://doi.org/10.1021/es051650b

Hijmans, R.J., Williams, E., & Vennes, C. (2017). geosphere. R package version 1.5-7.

Huete, A., Didan, K., Miura, T., Rodriguez, E.P., Gao, X., & Ferreira, L.G. (2002). Overview of the radiometric and biophysical performance of the MODIS vegetation indices. *Remote Sensing of Environment,* 83, 195-213. https://doi.org/10.1016/S0034-4257(02)00096-2

Kopec, B.G., Feng, X., Michel, F.A., & Posmentier, E.S. (2016). Influence of sea ice on Arctic precipitation. *PNAS,* 113(1), 46-51. https://doi.org/10.1073/pnas.1504633113

Lacroix, M.P., Prowse, T.D., Bonsal, B.R., Duguay, C.R., & Ménard, P. (2005). *River Ice Trends in Canada.* Paper presented at the 13th Workshop on the Hydraulics of Ice Covered Rivers, Hanover, NH.

Lawrence, D.M., Slater, A.G., Tomas, R.A., Holland, M.A., & Deser, C. (2008). Accelerated Arctic land warming and permafrost degradation during rapid sea ice loss. *Geophysical Research Letters,* 25, L11506. https://doi.org/10.1029/2008GL033985

Lehner, B., & Grill, G. (2013). Global river hydrography and network routing: baseline data and new approaches to study the world's large river systems. *Hydrological Processes,* 27, 2171-2186. https://doi.org/10.1002/hyp.9740

Libiseller, C., & Grimvall, A. (2002). Performance of partial Mann-Kendall tests for trend detection in the presence of covariates. *Environmetrics,* 13(1), 71-84. https://doi.org/10.1002/env.507

Lonergan, S., Difrancesco, R., & Woo, M. (1993). Climate change and transportation in northern Canada: an integrated impact assessment. *Climate Change,* 24, 331-351. https://doi.org/10.1007/BF01091854

Magnuson, J.J., Robertson, D.M., Benson, B.J., Wynne, R.H., Livingstone, D.M., Arai, T., et al. (2000). Historical Trends in Lake and River Ice Cover in the Northern Hemisphere. *Science,* 289, 1743-1746. https://doi.org/10.1126/science.289.5485.1743

Mantua, N.J., Hare, S.R., Zhang, Y., Wallace, J.M., Francis, R.C. (1997). A Pacific interdecadal climate oscillation with impacts on salmon production. *Bulletin of the American Meteorological Society,* 78, 1069-1079. https://doi.org/10.1175/1520-0477(1997)078%3C1069:APICOW%3E2.0.CO;2

Marchetto, A. (2017). rkt. R package version 1.5.

Meier, W.N., Stroeve, J., & Fetterer, F. (2007). Whither Arctic sea ice? A clear signal of decline regionally, seasonally, and extending beyond the satellite record. *Annals of Glaciology,* 46, 428-434. https://doi.org/10.3189/172756407782871170

Milburn, D., & Prowse, T.D. (2000). Observations on Some Physical-Chemical Characteristics of River-Ice Breakup. *Journal of Cold Regions Engineering,* 14(4), 214-223. https://doi.org/10.1061/(ASCE)0887-381X(2000)14:4(214)

Muhammad, P., Duguay, C., & Kang, K.K. (2016). Monitoring ice break-up on the Mackenzie River using MODIS data. *The Cryosphere,* 10, 569-584. https://doi.org/10.5194/tc-10-569-2016

Niebauer, H.J. (1988). Effects of El Nino-Southern Oscillation and North Pacific Weather Patterns on Interannual Variability in the Subarctic Bering Sea. *Journal of Geophysical Research,* 93(C5), 5051-5068.

Pavelsky, T.M., & Smith, L.C. (2004). Spatial and temporal patterns in Arctic river ice breakup observed with MODIS and AVHRR time series. *Remote Sensing of Environment,* 93, 328-338. https://doi.org/10.1016/j.rse.2004.07.018

Pearson, K. (1896). VVI. Mathematical contributions to the theory of evolution.—III. Regression, heredity, and panmixia. *Proceedings of the Royal Society of London*, 253-318. https://doi.org/10.1098/rsta.1896.0007

Prowse, T.D., Bonsal, B.R., Duguay, C.R., & Lacroix, M.P. (2007). River-ice break-up/freeze-up: a review of climatic drivers, historical trends, and future predictions. *Annals of Glaciology,* 46, 443-451. https://doi.org/10.3189/172756407782871431

Prowse, T.D., Furgal, C., Chouinard, R., Melling, H., Milburn, D., & Smith, S.L. (2009). Implications of Climate Change for Economic Development in Northern Canada: Energy, Resource, and Transportation Sectors. *Ambio,* 38(5), 272-281. https://doi.org/10.1579/0044-7447-38.5.272

River Ice Processes. (2017). Presented at the American Water Resources Association Alaska Section, Anchorage, AK.

Rokaya, P., Budhathoki, S., & Lindenschmidt, K. (2018). Trends in the Timing and Magnitude of Ice-Jam Floods in Canada. *Scientific Reports,* 8:5835. https://doi.org/ 10.1038/s41598-018-24057-z

Schmidt, D.F., Grise, K.M., & Pace, M.L. (2019), High-frequency climate oscillations drive ice-off variability for Northern Hemisphere lakes and rivers. *Climate Change.* https://doi.org/10.1007/s10584-018-2361-5

Scrimgeour, G.J., Prowse, T.D., Culp, J.M., & Chambers, P.A. (1994). Ecological effects of river ice break-up: a review and perspective. *Freshwater Biology,* 32, 261-275. https://doi.org/10.1111/j.1365-2427.1994.tb01125.x

Serreze, M.C., Holland, M.M., & Stroeve, J. (2007). Perspectives on the Arctic's Shrinking Sea-Ice Cover. *Science,* 315(5818), 1533-1536. https://doi.org/10.1126/science.1139426

Sewall, J.O. (2005). Precipitation Shifts over Western North America as a Result of Declining Arctic Sea Ice Cover: The Coupled System Response. *Earth Interactions,* 9. https://doi.org/10.1175/EI171.1

Shiklomanov, A.I., Lammers, R.B., & Vörösmarty, C.J. (2002). Widespread decline in hydrological monitoring threatens Pan-Arctic Research. *EOS, Transactions, American Geophysical Union,* 83(2), 13-17. https://doi.org/10.1029/2002EO000007

Sinnott, R.W. (1984). Virtues of the Haversine. *Sky and Telescope* 68(2).

Spearman, C. (1904). The Proof and Measurement of Association between Two Things. *The American Journal of Psychology,* 15(1), 72-101. https://doi.org/10.2307/1412159

Stephenson, S.R., Smith, L.C., & Agnew, J.A. (2011). Divergent long-term trajectories of human access to the Arctic. *Nature Climate Change,* 1, 156-160. https://doi.org/10.1038/nclimate1120

Trenberth, K.E. (1976). Spatial and temporal variations of the Southern Oscillation. *Quarterly Journal of the Royal Meteorology Society,* 102, 639-653.

Vermote, E., Wolfe, R. (2015a). *MOD09GQ MODIS/Terra Surface Reflectance Daily L2G Global 250m SIN Grid V006*. NASA EOSDIS LP DAAC. https://doi.org/10.5067/MODIS/MOD09GQ.006

Vermote, E., Wolfe, R. (2015b). *MOD09GA MODIS/Terra Surface Reflectance Daily L2G Global 1km and 500m SIN Grid V006*. NASA EOSDIS LP DAAC. https://doi.org/10.5067/MODIS/MOD09GA.006

Wallace, J.M., & Gutzler, D.S. (1981). Teleconnections in the geopotential height field during the Northern Hemisphere winter. *Monthly Weather Review,* 109, 784-812. https://doi.org/10.1175/1520-0493(1981)109%3C0784:TITGHF%3E2.0.CO;2

Yamazaki, D., Ikeshima, D., Tawatari, R., Yamaguchi, T., O'Loughlin, F., Neal, J.C., et al. (2017). A high-accuracy map of global terrain elevations. *Geophysical Research Letters,* 44(11), 5844-5853. https://doi.org/10.1002/2017GL072874

Yang, X., Pavelsky, T., & Allen, G. (*in review*). The past and future of global river ice. *Nature.*